THIS MANUSCRIPT HAS BEEN AUTHORED BY UT-BATTELLE, LLC UNDER CONTRACT NO. DE-AC05-00OR22725 WITH THE U.S. DEPARTMENT OF ENERGY. THE UNITED STATES GOVERNMENT RETAINS AND THE PUBLISHER, BY ACCEPTING THE ARTICLE FOR PUBLICATION, ACKNOWLEDGES THAT THE UNITED STATES GOVERNMENT RETAINS A NON-EXCLUSIVE, PAID-UP, IRREVOCABLE, WORLDWIDE LICENSE TO PUBLISH OR REPRODUCE THE PUBLISHED FORM OF THIS MANUSCRIPT, OR ALLOW OTHERS TO DO SO, FOR UNITED STATES GOVERNMENT PURPOSES. THE DEPARTMENT OF ENERGY WILL PROVIDE PUBLIC ACCESS TO THESE RESULTS OF FEDERALLY SPONSORED RESEARCH IN ACCORDANCE WITH THE DOE PUBLIC ACCESS PLAN (HTTP://ENERGY.GOV/DOWNLOADS/DOE-PUBLIC-ACCESS-PLAN).

MELT POOL MONITORING FOR CONTROL AND DATA ANALYTICS IN LARGE-SCALE METAL ADDITIVE MANUFACTURING

B.T. Gibson*, Y.K. Bandari°, B.S. Richardson*, A.C. Roschli*, B.K. Post*, M.C. Borish*, A. Thornton†, W.C. Henry†, M. Lamsey‡, L.J. Love*

*Oak Ridge National Laboratory, Manufacturing Demonstration Facility, 2370 Cherahala Blvd, Knoxville, TN 37932
° EWI - Buffalo Manufacturing Works, Buffalo, NY, 14203, USA
† GKN Aerospace, Hazelwood, MO, 63042, USA
‡ University of Tennessee, Knoxville, TN, 37996, USA

Abstract

Laser-wire based Directed Energy Deposition (DED) processes are being developed at Oak Ridge National Laboratory's Manufacturing Demonstration Facility, in collaboration with GKN Aerospace, for large volume metal additive manufacturing of metallic structures. The technology has the potential to deliver reduced costs and lead times when compared to conventional methods of manufacturing in several industries. While complex structures are being produced with relatively high deposition rates and at near-net shape, issues persist with achieving consistent geometric accuracy and thermal stability. A significant research effort is focused on developing coordinated, multi-modal sensing and control for addressing these issues. An introduction to this large-volume metal process will be provided, followed by investigations into real-time thermal monitoring capabilities that support control and data analytics frameworks. Studies focused on melt pool monitoring via infrared thermography, thermal and geometric effects on melt pool size measurement, and interactions between process variables and thermal monitoring metrics are presented.

Introduction

Large-scale metal additive manufacturing (AM), also known as metal Big Area Additive Manufacturing (m-BAAM) technologies are garnering increased attention in several industries due to the potential for reduced costs and lead times when compared to traditional methods of manufacturing certain components. In the aerospace industry, a driver for adoption of large-scale AM technologies is the high buy-to-fly ratio (commonly 10:1, or worse) in the production of Titanium aerostructures, traditionally machined from large forgings, which generates significant material scrap. Directed energy deposition (DED) is a family of AM technologies being explored for this application, with a focus on laser-wire based technologies for production of tailored pre-forms for Ti-6Al-4V components. The central challenge in m-BAAM however is simultaneous control of geometry, material properties, and residual stress and distortion. Methods being utilized in process development to address this challenge include predictive process modeling, real-time sensing and control, post-build characterization, and data analytics. In particular, real-time sensing and control offers the ability to control bead geometry (width or height) which can vary due to thermal conditions that are dependent on geometry, tool path, interlayer time, etc. and also detect undesired conditions in the build process and make corrective adjustments to deposition parameters. Much research has been focused on incorporation of sensors in DED for imaging the

melt pool and resulting bead geometry; however, the literature is heavily weighted toward laser-powder DED processes rather than laser-wire DED processes. Issues of scale between powder and wire-based process and characterization of unique interactions between process variables and melt pool size measurements in laser-wire based DED make the present research necessary to address the knowledge gap.

In terms of the literature that is available on laser-wire based DED processes, Heralic et al. have been major contributors to sensing and control system development, incorporating camera systems in the robotic print head that include a CCD-based camera for seam tracking and a CMOS camera for weld pool imaging [1]. CCD-based cameras have been widely utilized in a variety of manufacturing processes for monitoring and control purposes. Sentenac et al. characterized the performance of a low-cost CCD-based camera, utilized for both temperature and displacement measurements, as operating temperature varied over a relatively large range. Models and compensation methods were developed to ensure the accuracy of the detector [2]. Medrano et al. presented the development of a system for laser-wire based DED and compared infrared pyrometers for off-axis, real-time monitoring of the rear of the melt pool and the substrate, or previously deposited layer, ahead of the melt pool. The system had a capacity for 2 kW of laser power. Temperature measurement range, response time, accuracy, and sensor construction (integrated optics and electronics versus separate housing of the components) were shown to be factors in selecting the ideal sensors for the application. Positioning and aiming of the pyrometer and the potential for wire masking, or the blocking of the point-of-interest on the workpiece from the pyrometer's view due to the wire and/or wirefeeder during omnidirectional printing, were discussed as critical issues [3]. In general, in-axis cameras are preferred for monitoring laser welding and related processes; ref [4] is an example from laser keyhole welding. A dichroic mirror is utilized to reflect the fiber laser beam in the laser optics while transmitting the emission wavelengths of interest for sensing. Secondary illumination sources, such as lasers or LEDs that emit wavelengths in the range of sensing, are commonly used as well.

Beyond laser welding, other related processes from which sensing and control knowledge can be gained include laser-powder based DED, laser cladding (a form of laser-powder based DED), and Electron Beam Freeform Fabrication; furthermore, in-situ monitoring of the melt pool with visible or infrared cameras is a topic of significant research across an even broader variety of additive manufacturing process and has proven repeatedly to be critical for ensuring part quality; ref [5] provides one such example in a laser powder bed fusion process. In laser cladding, Bi at al. evaluated various sensors for monitoring the infrared emissions from the melt pool, with the ultimate goal of guiding sensor selection for process control. Sensors included a photodiode, a pyrometer, and a CCD-based camera. A dependence of the emitted signals on the primary process parameters was evident, and the signals also correlated with clad results, such as geometry and dilution [6]. Hu et al. developed a system for laser cladding with a 1 kW laser and a co-axially mounted melt pool imager based on a CCD camera. Images acquired with the camera were used as feedback for a closed-loop control system, but the authors discuss several monitoring-centric issues encountered in system development. In particular, the virtues of co-axially mounting the camera are outlined, which addresses limited observation space due to the short nozzle to substrate distance in powder-DED, image distortion due to viewing angle, and interference from laser light intensity and powder streams. Selection of the proper IR filter, laser wavelength filter, and iris aperture were discussed as well [7]. In a unique approach, Meriaudeau et al. developed a thermal monitoring system for laser cladding to measure the temperature of the melt pool and infer

variations in the mass flow rate of powder based on temperature measurement fluctuations, according to the Beer-Lambert law, which relates attenuation of light to the properties of the medium through which it is travelling. The system utilized a CCD-based camera, and a second CCD-based camera was also used to obtain geometric measurements of the deposit. The authors claim the signals obtained from the imaging systems would allow for process optimization and closed-loop control [8]. In the Electron Beam Freeform Fabrication (EBF^3) process, which is a form of wire-fed DED, Zalameda et al. describe the calibration of a near infrared (NIR) camera for off-axis, real-time monitoring of temperatures of the melt pool and solidification zone. Additionally, image analysis techniques were utilized to test the feasibility of thermally-based non-destructive evaluation (NDE) being applied to determine the quality of deposits. The CCD-based camera utilized in the study was calibrated using a radiometric characterization technique with a calibrated blackbody radiation source. The camera was positioned at an angle 60 degrees from the molten pool, opposite the wire feeder, and intensity values were used to delineate between the molten pool and the solidification zone directly trailing the molten pool. Wire masking was discussed as a pertinent issue to consider in camera positioning and aiming. Authors discussed using the acquired image data to both create a closed-loop system for controlling deposition parameters and conducting thermal NDE with pre-located defects in the substrate [9].

In laser-powder based DED, Griffith et al. characterized thermal gradients using two non-invasive techniques, infrared imaging for bulk temperature measurements and thermal gradients in the build and high speed visible imaging to measure the melt pool and it's corresponding thermal gradients. The limitations of making absolute temperature measurements for an object under construction with no known emissivity was discussed; as such, relative measurements were made. Agreement was observed between thermal gradients in and immediately adjacent to the melt pool characterized with high speed visible imaging and bulk infrared data obtained near the melt pool region. The possibility for data correlation with microstructure evolution and exploitation of relationships for feedback control purposes was discussed [10]. Alternatively, Hofmeister et al. used visible light radiation pyrometry to monitor the molten pool in laser-powder based DED. A high speed digital camera with filtering to remove the laser radiation was mounted in-axis to image the molten pool, and relationships between absorbed energy and pool geometry (width, length, and isotherm area) were determined. These relationships were found to be smooth, consistent, and suitable for exploitation via closed loop process control [11]. Hofmeister et al. also used thermal imaging of the laser-powder DED process to characterize the length scale of the molten zone and corresponding cooling rates. Imaging was accomplished with an in-axis CCD-based camera system measuring at 650 nm, sufficiently below the laser wavelength of 1064 nm [12].

In addition to closed-loop control, monitoring of the melt pool and corresponding thermal gradients and cooling rates in DED has been important for model validation. Hu and Kovacevic used a dual camera system to monitor the melt pool for validation of a finite element model in laser-powder based DED. A CCD-based camera with filtering to image in the near-infrared (NIR) range and block laser wavelengths was used to obtain a melt pool image and establish an isotherm of the melting point temperature. A second high speed camera with shuttering and a synchronized illuminating laser was used to verify the position of the edge of the molten zone [13]. Aggarangsi et al. used numerical modeling and a process map approach to predict transient changes in the melt pool size in laser-powder based DED. Results of this approach were compared against experimental measurements obtained with a thermal imaging system during a laser power step change. Melt pool sizes were on the order of < 1 mm^2, and the difficulty in measuring response

times experimentally was highlighted [14]. Aggarangsi et al. also used observations from thermal monitoring of laser-powder based DED as motivation to develop and model laser power reduction schedules as a method of melt pool size management when depositing near a free edge [15]. Along the same lines, Beuth and Klingbeil outlined modeling and process mapping-based research aimed at determining the influence of primary process parameters on deposition characteristics, such as melt pool geometry, in laser-powder based DED [16]. Finally, on the issue of process scale, Birnbaum et al. applied a modeling and process mapping approach to scale predictions of melt pool length and wall thickness from a laser-powder based DED process with a maximum laser power of 500 W to a process with a laser power capacity of 2700 W [17].

The aim of the present research was to tailor a melt pool monitoring system to the laser-wire DED process for m-BAAM, allow for consistent real-time melt pool size measurement, and to characterize interactions between primary process variables (laser power, wire feed rate, print speed) and melt pool size. Additionally, toolpath-dependent intralayer and interlayer trends in melt pool size were examined, along with the effect of wire masking of the melt pool and compensation of the same. These issues were addressed with the goal of supporting a reliable closed-loop melt pool size control system.

Methods

Depositions in the present work were printed in a custom, laser-wire DED work cell that contains an industrial 6-axis robot, wirefeeder, and hot wire system, with a print head that houses laser optics, directing power from two 10 kW fiber delivered diode lasers that are combined into a single fiber. Nominal deposition parameters for the majority of studies presented are shown in Table 1. All studies were conducted with 1.6 mm diameter Ti-6Al-4V wire; a 39° wire lead angle was used along with a 6° laser lead angle. Wire feed orientation (front, back, side) varied on a case by case basis and is specified in the methods or results for each individual study.

Table 1: Primary Process Parameters

Parameter	*Value*	*Units*
Delivered Laser Power	8.71	kW
Deposition Rate	2.4	kg/hr
Print Speed	8	mm/s
Hot Wire Power	370	W

Deposition rate is a function of wire speed, wire diameter, and wire density, which for Ti-6Al-4V was assumed to be 4.43 g/cm^3. Delivered laser power, as opposed to commanded power, was determined through a calibration process that utilizes a power puck; absorbed power is a function of thermal transfer efficiency and was not characterized within the scope of this work. Printing was completed in an Argon environment that was established using a tent that enclosed the build volume. Argon flow is provided to the tent to purge and maintain Oxygen levels below 300 ppm for the duration of the deposition process. Ti-6Al-4V build plates, 6.35 mm in thickness, were utilized.

Monitoring of the melt pool was accomplished with an in-axis thermal camera; details of the camera hardware are considered protected intellectual property (IP), and therefore certain

information has been withheld from this article. The laser beam was reflected in the optics using a dichroic mirror, allowing emissions from the melt pool to transmit through the optics to the camera. Sensing in the IR range was accomplished via filtering, below the range of laser wavelengths. Sensing near the visible range leads to less emissivity dependence in the measurement [18]. A temperature calibration curve for the camera was generated through a calibration procedure using a diode of known wavelength and emissivity, and a software package acquires and converts gray-scale images to false color images in real-time. Two sets of thermal camera optics were tested, which yielded different effective zooms. A secondary visible, in-axis camera was used for imaging the melt pool to identify wire input location and monitoring process stability.

Noise reduction in thermal imaging was accomplished through high-pass temperature filtering that established a temperature cut-off, below which temperature data was removed. This method reduces the measurement range of the camera but maintains measurement capability at an adequate range around the melting point of the material. A range of exposure rates were explored for imaging the melt pool, with the goal of allowing for adequate camera integration time without detrimentally limiting the frequency of image generation, which would be important for work on real-time sensing and closed-loop control that would follow. The melt pool was defined by thresholding the thermal field to generate a measurement of size; the specific thresholding methodology utilized is considered protected intellectual property. While there is a transition zone trailing the melt pool in which solidification occurs, significant effort was not directed at identifying the precise location and corresponding temperature of this transition; rather, an emphasis on measurement noise was taken in making slight adjustments to the thresholding method, the goal being to establish a low-noise, melt pool definition that tracks consistently with total melt pool size and the thermal properties of the build.

To attain calibrated measurements of melt pool size, two methods were utilized. Thermal field images of the melt pool were compared to images of the solidified bead terminus on single bead-on-plate depositions, and the wire, an object of known size, was examined in thermal images.

To establish an understanding of melt pool size behavior in laser-wire DED it was important to isolate and study the interactions of melt pool size with the three primary process variables of print speed, laser power, and wire feed rate. Step changes of each parameter were commanded during single, bead-on-plate depositions while monitoring with the thermal camera. Response time was then examined. Time intervals between step changes were considered to be sufficiently long to allow for the response time to steady-state to be characterized. A further examination of bandwidth was not part of this scope of work; a preliminary examination has been presented in ref [19]. Print speed was varied from its nominal value of 8 mm/s to 4 mm/s and then 12 mm/s. Laser power was varied from its nominal value of 8.71 kW to 10 kW and then back to 8.71 kW. Wirefeed rate was commanded 60% higher, from its nominal value of 75 mm/s, which corresponds to a deposition rate of 2.4 kg/hr, to a rate of 120 mm/s.

To examine melt pool size responses that are characteristic of part printing in laser-wire DED, within-layer and interlayer trends were studied in the printing of single-bead walls. Single-bead walls 175 mm long and 75 mm tall were printed with a layer height of 1.6 mm; nominal bead width was approximately 11.5 mm. Wire feed orientation was front-feed, with the exception of a bead termination routine which reversed the print head at the end of each bead to deposit additional material at the end of the wall; this routine was carried out for geometry control purposes, but it

also created a highly transient process region for which the melt pool size response could be characterized. Reversal distance, laser power, and wire feed rate can vary on a per layer basis during the termination routine, and the parameters used are listed in Table 2.

Table 2: Bead Termination Routine Parameters

Parameter	*Value*	*Units*
Initial Distance	10	mm
Distance Increment	1	mm
Laser Power Increment	-1	%
Wirefeed Increment	0	%
Maximum Layer	20	

A proprietary system for scanning the build geometry with a laser line scanner and adjusting printing parameters to maintain nominal layer height was utilized as well. Details of the system are considered protected intellectual property; therefore, limited details are presented here. However, it is noteworthy that the scanning process led to variable interlayer times during wall printing (longer interlayer time every three layers).

The final objective of the present work was to characterize, and consider compensation for, the wire masking effect. Wire masking is an effect in laser-wire DED in which the wire blocks the view of the melt pool from the camera or other sensor being used to take a measurement. This can lead to corrupted measurements of melt pool size that would negatively impact the performance of a closed-loop control system. This effect can be variable and toolpath-dependent in the case of print heads that do not rotate to maintain a consistent wire feed direction with toolpath. The degree to which this effect is present was characterized by printing a 16-sided, bead-on-plate polygon while translating the print head in the XY plane only (no rotation about the Z axis). The melt pool was monitored to determine the magnitude and angles at which masking occurs, and then a toolpath dependent compensation algorithm was developed and applied to the melt pool size measurement in post-processing to serve as an example of measurement corrections that are possible.

Results

High quality IR images of the melt pool were attained after proper selection of the temperature cutoff for high-pass filtering and the camera exposure rate. Figure 1 displays an example false-color image of the thermal field for a side-feed melt pool; image size is 218x164 pixels. The indication of the wire is visible at the top of the melt pool. The measurement range of the calibration curve is from 1250° C to 2507°C.

Figure 2 displays example thermal fields for a range of temperature cutoffs and exposure rates. With no high pass filtering, the melt pool is not clearly distinguishable from the background noise. A temperature cutoff in the range of 1200° C - 1300° C was found to be satisfactory. The images of varying exposure rates were from front-feed beads and with camera optics that yielded an increased zoom. The higher resolution image comes with a cost of truncating the tail of the melt pool, the amount of which depends on travel direction. At low exposure rates the laser spot, and to some degree the plasma plume, are more prominent features of the thermal field. Higher

exposure rates allowed for more integration time and better imaging of the melt pool. As expected, exposure rates that yielded quality images of the melt pool were also dependent upon the physical setting of the iris in the camera optics.

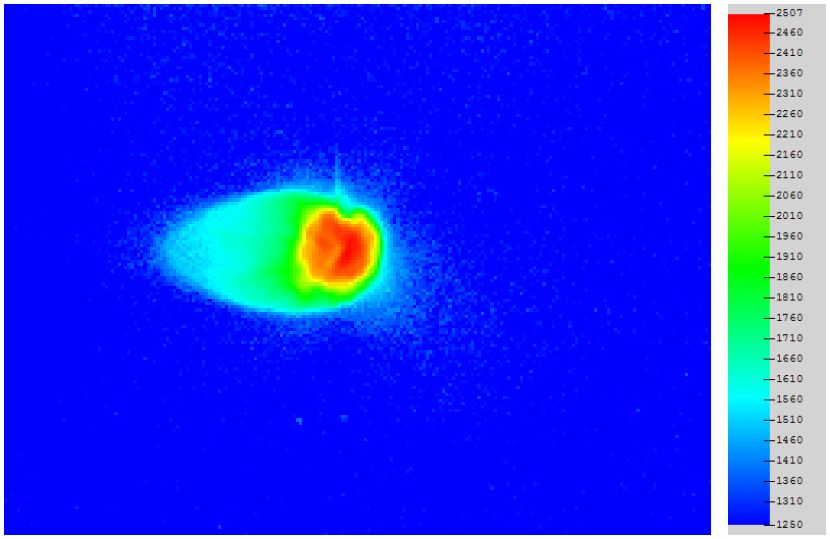

Figure 1: Typical Thermal Field for a Side-Feed Melt Pool

Given a satisfactory thermal field, the melt pool itself was defined using a thresholding method. Size was determined by a summation of pixels within the threshold. As stated in the previous section, emphasis was not placed on identifying the molten-to-solid transition zone, but rather identifying a low-noise definition of the melt pool that would track consistently with total melt pool size and the thermal properties of the build.

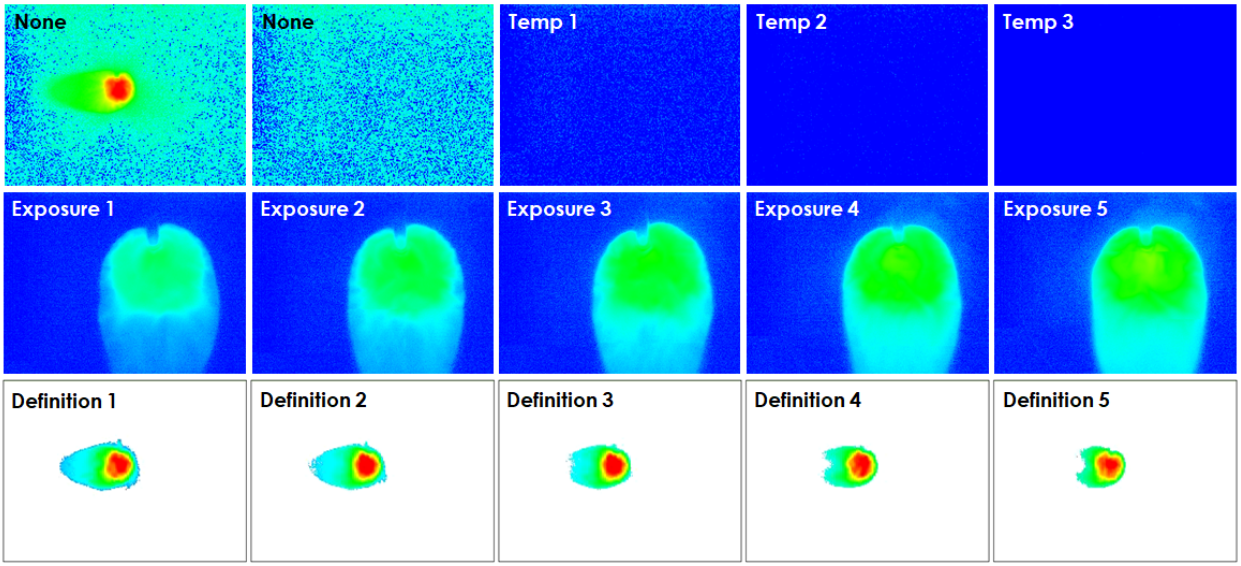

Figure 2: Thermal Fields with Varying Temperature Cutoffs for High-Pass Filtering (top row); Deposition Image with No Temperature Cutoff (top left); Deposition Thermal Fields for Varying Exposure Rates (middle row); Melt Pool Definitions using Varying Thresholding Methods (bottom row); Specific Values Removed to Protect IP

Figure 2 also displays an example of five different melt pool definitions. Pixels outside the melt pool boundaries have been removed from the images. The corresponding size measurements, from a bead-on-plate experiment, are shown in Figure 3. In Figure 3, melt pool size is plotted against image frame, which are logged at 12.5 Hz during deposition, a down-sampling of images that are available in real-time in the acquisition software at a rate that is considered protected IP.

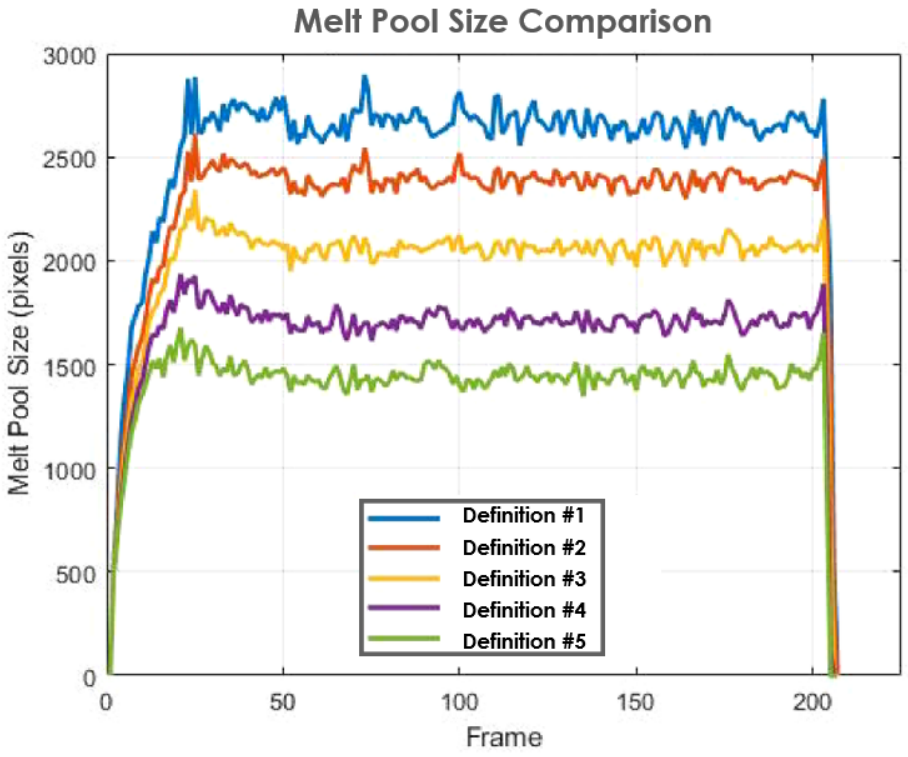

Figure 3: Melt Pool Size Measurements Resulting from the Application of Varying Thermal Field Thresholding Methods

Results indicate that noise reduction via thresholding method is attainable, as evidenced by a comparison of the signal noise of melt pool definitions 3 and 4, for example, with that of definition 1 in Figure 3. Low-noise melt pool definitions were selected for the experiments that follow.

The calibration of image size was determined through two methods and agreement between the methods was observed. Figure 4 displays the thermal field of the side-feed melt pool from Figure 1, alongside a photograph of the bead terminus. Also shown is the thermal field of a back-feed deposition, in which the wire is clearly visible. In the correlation of the side-feed melt pool length in the thermal image and the measured length in the bead terminus photograph, 67 pixels corresponds to 21 mm, or 0.313 mm/pixel. In examining the back-feed thermal image, it was found that the width of the wire was 5 pixels; given the actual wire width of 1.6 mm, this means a calibration of 0.32 mm/pixel. Averaging the two results yields a calibration of 0.317 mm/pixel or an area of approximately 0.1 mm^2 per pixel. Therefore, for a melt pool size of 2000 pixels, a typical order of magnitude for the melt pools in this study, the actual melt pool area would be approximately 200 mm^2.

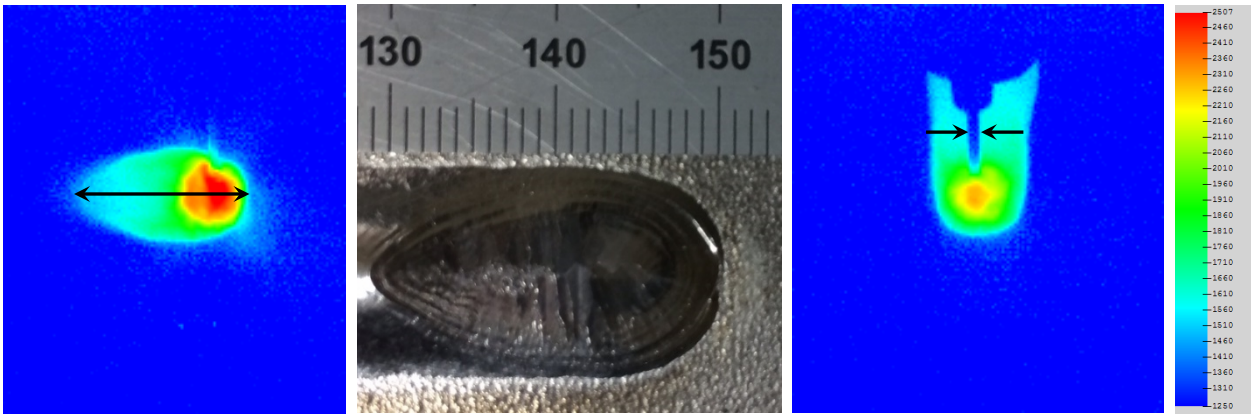

Figure 4: Thermal Field of Side-Feed Melt Pool, Photograph of Bead Terminus (units in mm), Thermal Field of Back-Feed Melt Pool (left to right)

Figure 5 displays the melt pool size response for step changes in print speed. The feed direction for this test was side-feed. The step change in speed from 8 mm/s to 4 mm/s resulted in a melt pool size increase of approximately 40%. An initial sharp increase in size was observed with a duration of approximately 2 seconds, followed by a slower rise to what was considered steady state that lasted approximately 4 seconds. Figure 6 displays the resulting bead geometry and the corresponding thermal images of the melt pool. The step change in speed from 4 mm/s to 12 mm/s resulted in a melt pool size decrease of approximately 44%. The size response was characterized by a sharp decrease with a slight overshoot compared to what would become the steady-state melt pool size. The initial decrease had a duration of approximately 1.6 seconds, and the time from overshoot to steady-state was approximately 1 second. The overshoot would suggest

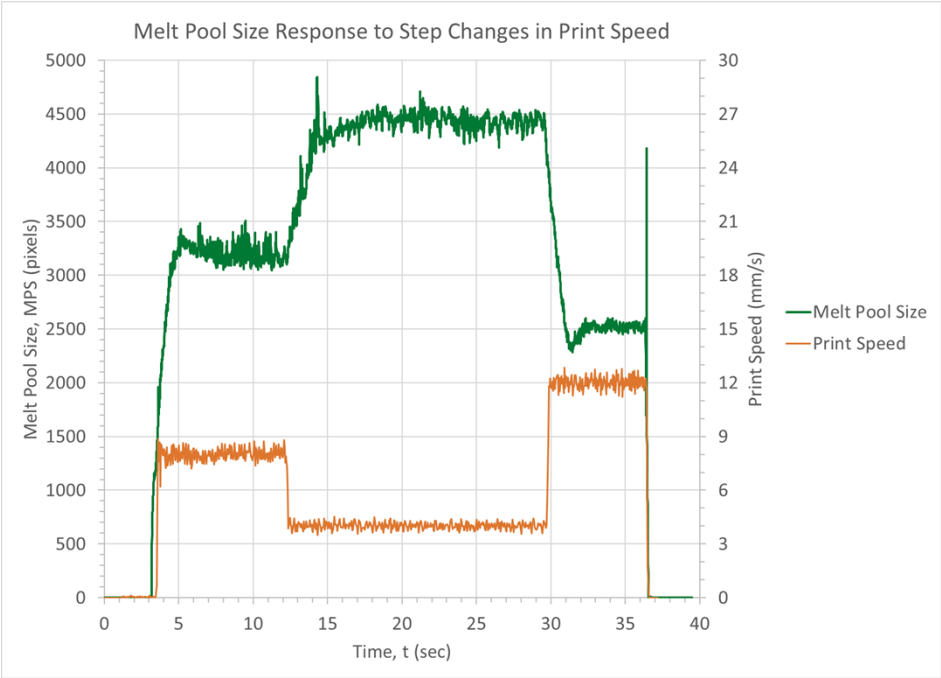

Figure 5: Melt Pool Size Response for Step Changes in Print Speed

that some necking would be present in the bead geometry, but this feature was not clearly evident upon visual inspection of the bead geometry.

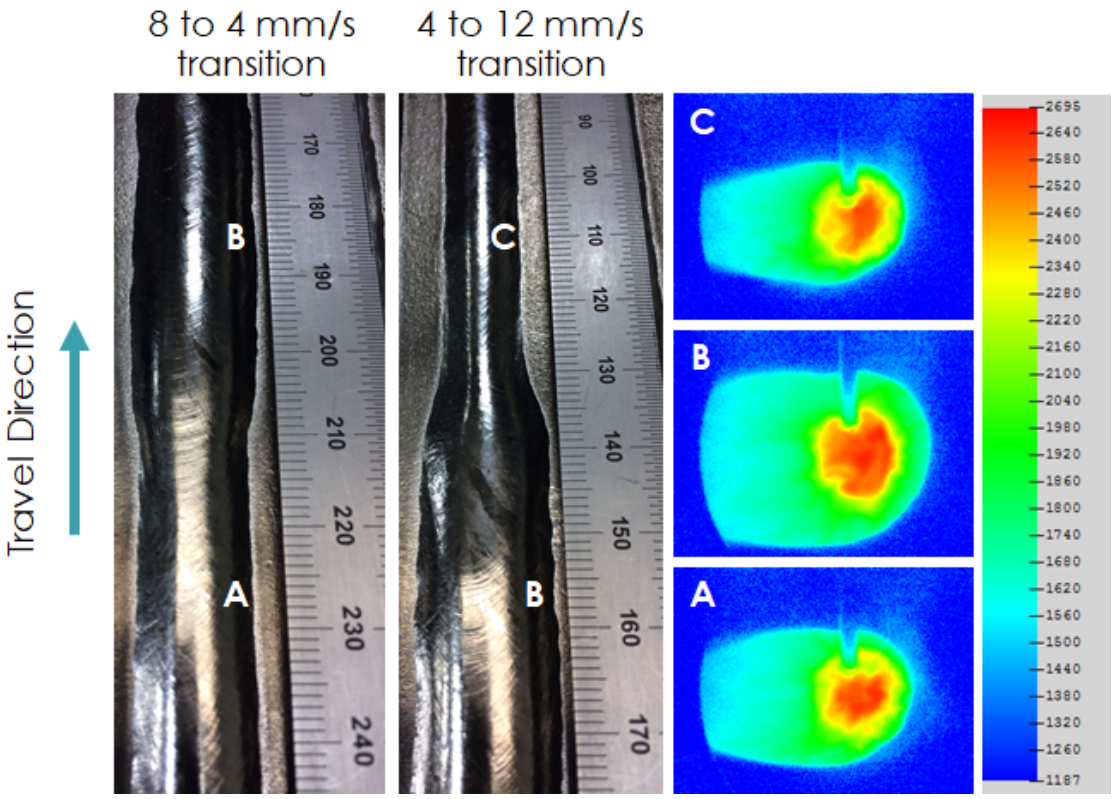

Figure 6: Bead Geometry and Thermal Images for Step Changes in Print Speed

Figure 7 displays the melt pool size response for step changes in laser power. The size response for a step change of 8.71 kW to 10 kW yielded an approximate 29% increase in size and was characterized by an initial sharp rise by a longer, slower increase to steady-state. The sharp rise had a short duration, and the slower increase occurred over a period of approximately 1.8 seconds. Similarly, the step change from 10 kW to 8.71 kW yielded a melt pool size response that was dual-phased, with an initial sharp decrease followed by a long, slow decrease to steady-state. The initial decrease was rapid, followed by an approximately 2 second long reduction in size. The melt pool size returned to approximately the same size that was observed for the initial section of 8.71 kW laser power. Also noteworthy was the initial fluctuation in melt pool size that occurred at bead initiation, although this behavior was not universally observed for all tests.

Figure 8 displays the melt pool size response for a step change in wire feed rate, or deposition rate. Wire feed rate was commanded 60% higher from its initial value of 75 mm/s, which corresponds to a deposition rate of 2.4 kg/hr, to a value of 120 mm/s. This magnitude of an increase was found to be higher than what was sustainable, i.e. the wire feed drive tension was set to allow for some slippage to avoid tripping the wirefeeder in overload situations, and so instead, a self-limiting wire feed maximum was observed. The self-limiting maximum was observed to be 93.4 mm/s on average, a 24.5% increase compared to nominal. However, a dynamic response was also observed in which the wire feed rate briefly attained the 60% increase before decaying to the

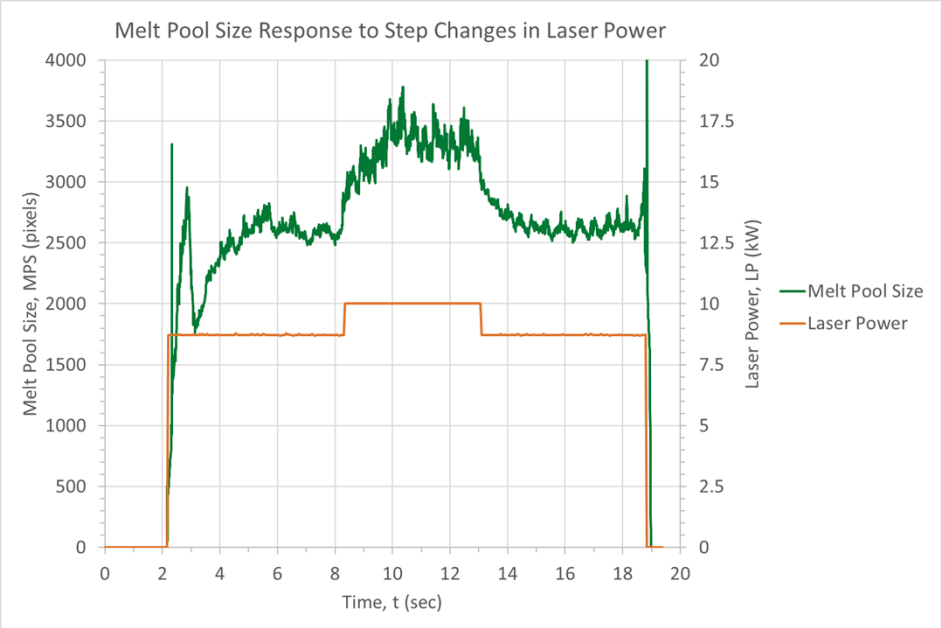

Figure 7: Melt Pool Size Response for Step Changes in Laser Power

self-limiting maximum. This dynamic response induced a corresponding fluctuation in the melt pool size. It is established in the literature that the action of increasing the feed rate of a lower temperature feedstock into an established melt pool will cause the melt pool to contract in size. This was observed in the dynamic response, an approximate 17% reduction in size, and for the steady-state response at the self-limiting maximum wire feed rate, an approximate 2% reduction in size. It must be noted however that this experiment was conducted in the front feed orientation and with the thermal camera optics with a greater zoom, which led to the tail of the melt pool being truncated, as seen in Figure 8. A consequence is that the size reduction percentages are less than

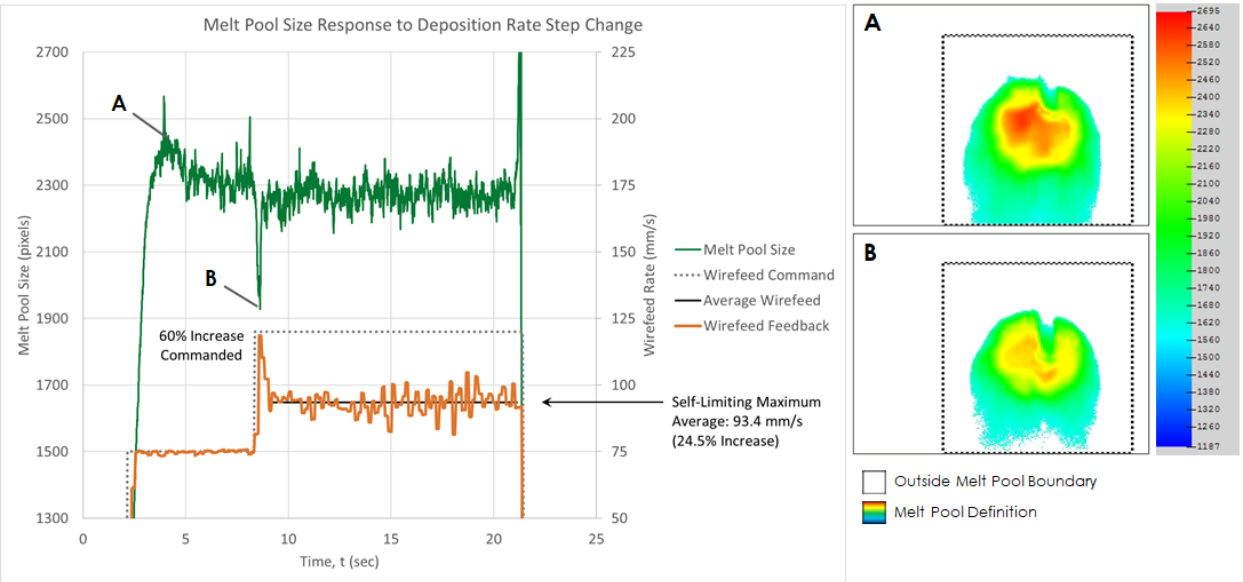

Figure 8: Melt Pool Size Response for a Step Change in Wire Feed Rate

what they would have been if the entire melt pool had been visible. Greater reductions in the measured size likely would have been recorded if the entire melt pool had been imaged. Despite the limited field of view however, the contraction of the melt pool during the dynamic response of wire feed rate was still observable; this is highlighted in Figure 8, inset B.

The within-layer, or intralayer, trend for melt pool size for a typical layer of a single bead wall, along with select melt pool images and a wall photograph, are shown in Figure 9. Bead initiation is typically characterized by some material build-up, which is a function of, among other things, the timing at which the wire begins to feed into the established melt pool. This is reflected in the melt pool size measurement as an increase in size at the beginning of the bead, followed by a reduction to what can be considered steady-state, although there are slight fluctuations present. There is then a significant increase in melt pool size as the deposition proceeds through the bead termination routine, which results in a large bulb of material deposited at the end of the wall, as seen in Figure 9. This general trend was consistent for each layer of the single bead wall, although there were evolutions in the magnitude of the melt pool size observed in bead initiation and the termination routine, with the magnitude generally increasing as layer number increased.

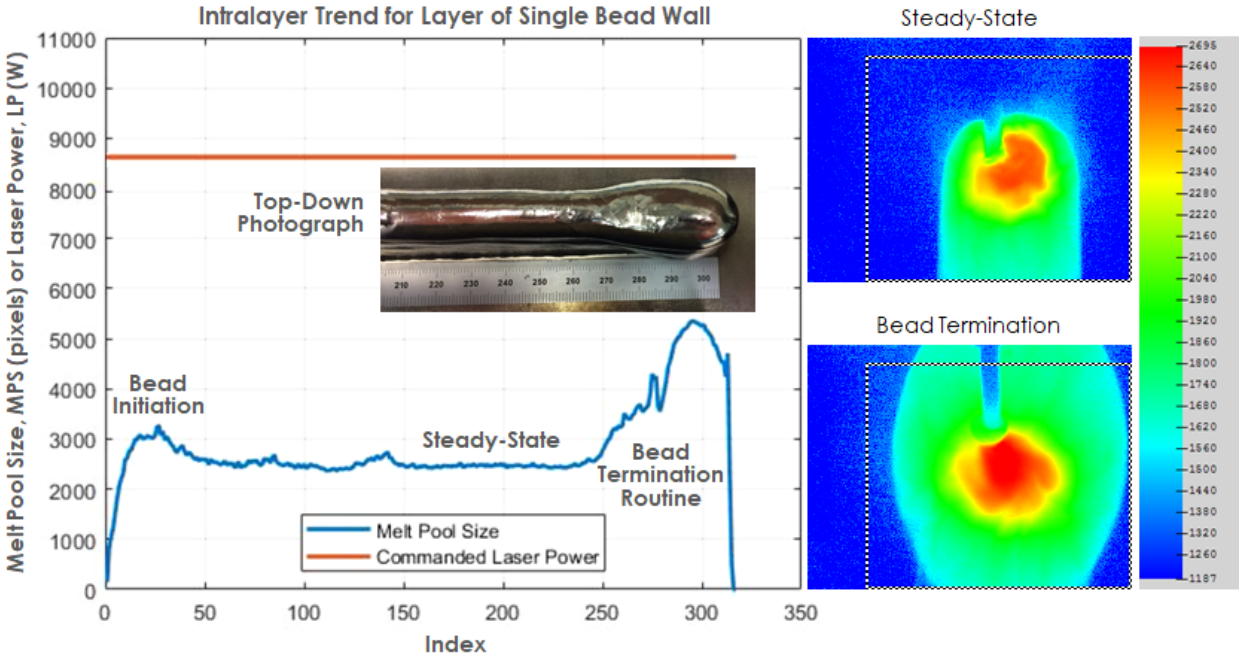

Figure 9: Intralayer Trend for Layer of Single Bead Wall

Figure 10 displays the interlayer trend in melt pool size for the single bead wall. With the exception of layer 1, the plot is color-coded per groupings of 3 layers, between which geometry scans were completed. The melt pool size trend shows a decrease over the initial layers, followed by an upward trajectory, with a sawtooth-like waveform, likely induced by the unique sequence of interlayer times. After increasing, the melt pool size reaches a relatively consistent magnitude, followed by a very slight decrease in the final layers of the wall. The initial decrease in melt pool size was reflected in a scan of final wall geometry. Figure 11 displays the YZ mid-plane profile for the single bead wall, which shows a narrowing of wall width following the first layer, and the cross-section would indicate that several layers were deposited before the width recovered to that

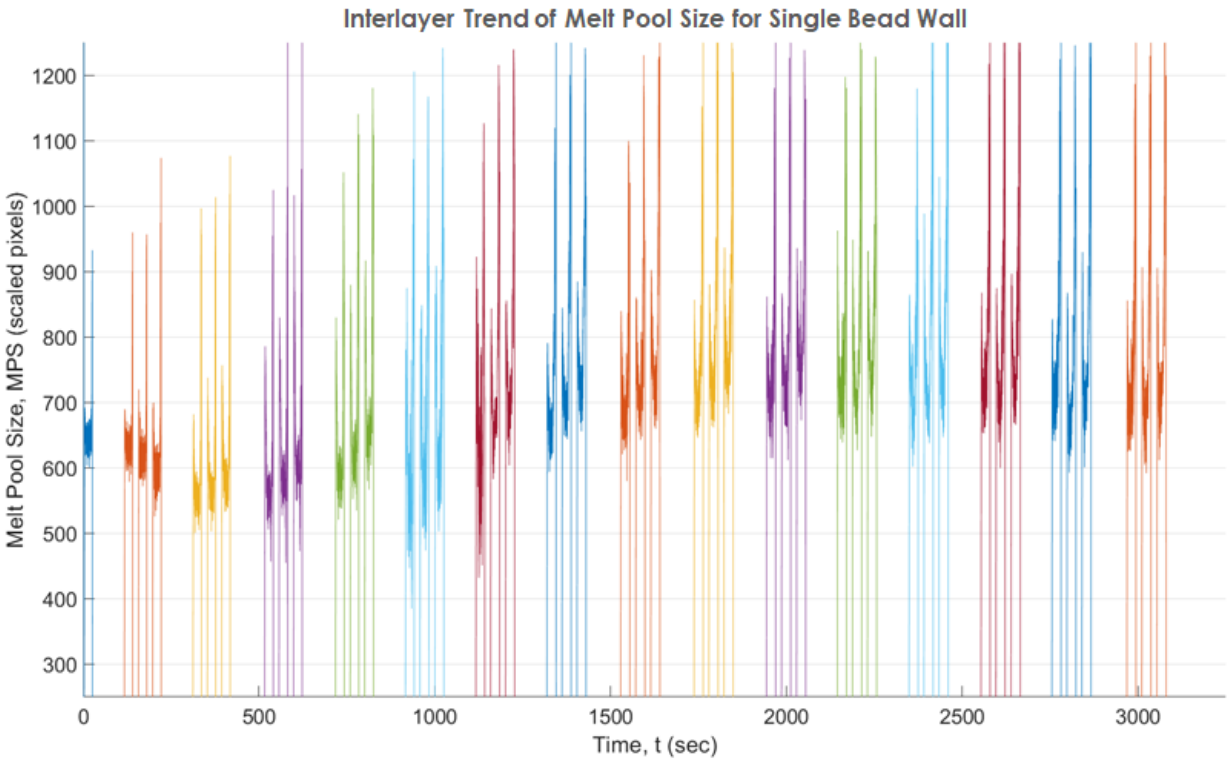

Figure 10: Interlayer Trend of Melt Pool Size for a Single Bead Wall

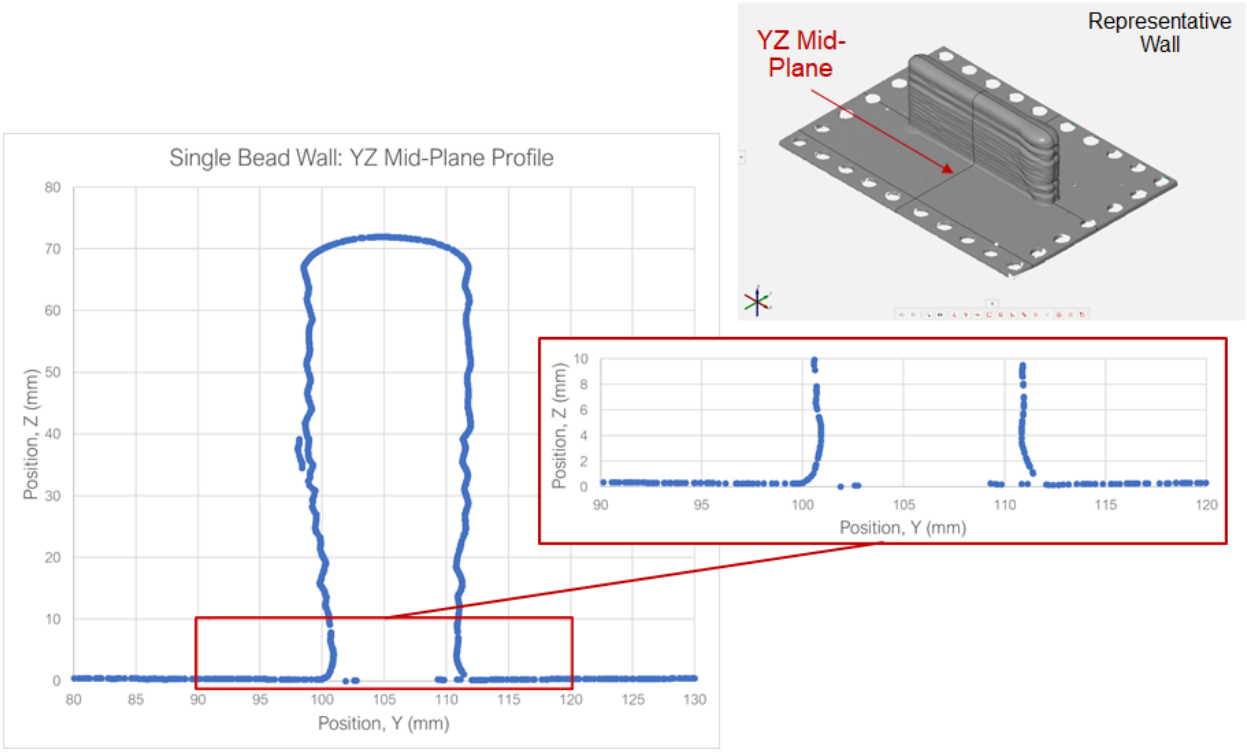

Figure 11: YZ Mid-Plane Profile for Single Bead Wall

of layer 1. It is believed that this behavior, as opposed to a monotonic increasing of wall width, as might be expected due to thermal properties of the build, is driven by a geometric effect, the influence of which outweighs the thermal effect in the initial layers of the print. This geometric effect may be driven in part by variations in wetting angle, which would be influenced by bead-on-bead deposition as opposed to bead-on-plate deposition, which is the case for layer 1. This is an issue worthy of further investigation.

The results of the wire masking test are shown in Figures 12 and 13. Primary process parameters were adjusted slightly for this test to 6.53 kW laser power, a 6mm/s print speed, and a 1.8 kg/hr deposition rate. Images of the melt pool are shown in Figure 12 for each deposition angle in the 16-sided polygon (a 22.5° resolution). Figure 13 displays the uncompensated melt pool size trend, in which there was a significant decrease due to wire masking. The melt pool size measurement was reduced by a factor of approximately 8.5% at maximum masking.

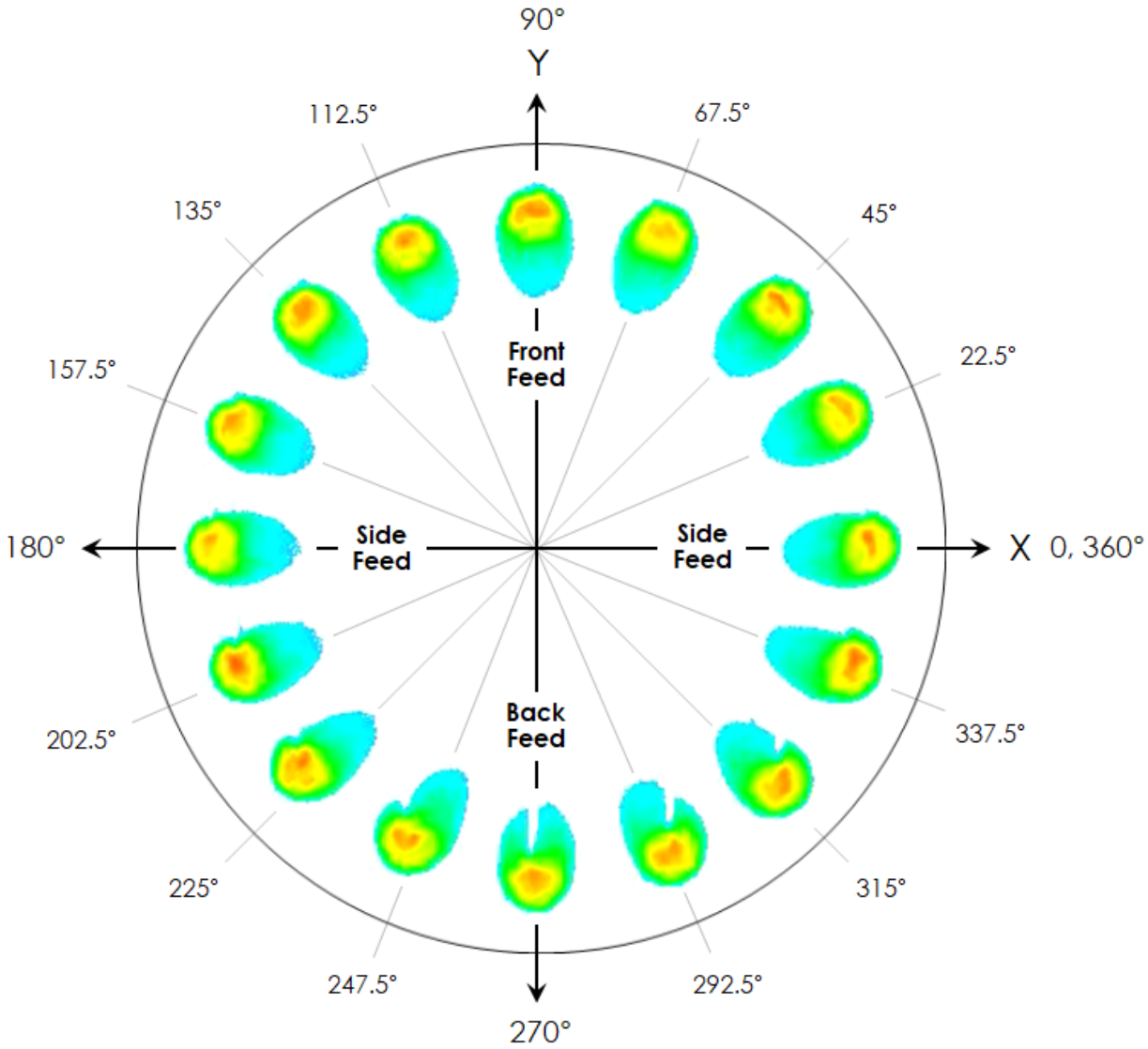

Figure 12: Melt Pool Images for Wire Masking Test, Displayed per Deposition Direction

A reduction of some amount occurred over the range of deposition angles from 202.5° to 337.5°, in which there were noticeable features in the melt pool shape, caused by the wire, shown in Figure 12. As stated previously, this masking effect could corrupt measurements of melt pool size that would negatively impact the performance of a closed-loop control system.

A compensation algorithm was developed as a demonstration of a measurement correction that could be applied to account for the wire masking effect. The algorithm applied a magnitude adjustment factor in post-processing that was deposition angle dependent; further details are considered proprietary and have been withheld to protect intellectual property. The resulting melt pool size measurement with wire masking compensation is plotted in Figure 13 as well. Application of the algorithm resulted in a smooth (apart from measurement noise) melt pool size trend that was free from influence of wire masking and varied only due to thermal effects and subtle changes in melt pool size/shape that are dependent on deposition direction.

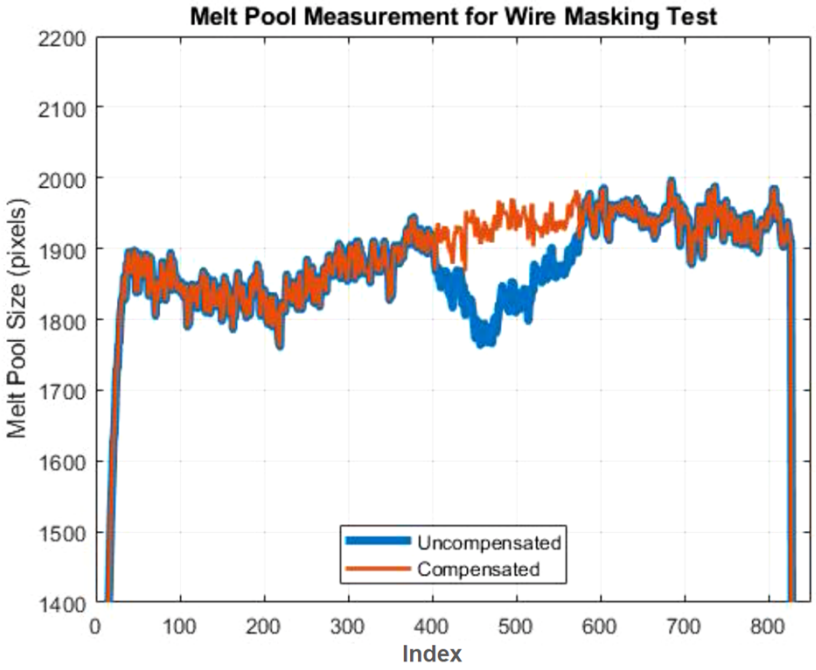

Figure 13: Melt Pool Size Measurement for Wire Masking Test, With and Without a Compensation Algorithm Applied

Discussion and Conclusions

The goal of this work was to demonstrate consistent real-time melt pool size measurement, characterize interactions between primary process variables (laser power, wire feed rate, print speed) and melt pool size, and to investigate the wire masking effect, specifically for laser-wire based DED, a process that is underrepresented in the literature compared to laser-powder based DED. These issues were also addressed with the goal of supporting reliable closed-loop melt pool size control. Camera and software settings were determined that yielded high-quality images of the melt pool thermal field, and images were processed to define the melt pool size. Much work in the literature has been focused on defining the melt pool boundary or finding the location, or the temperature, of the molten-to-solid transition zone immediately trailing the melt pool. Instead,

in this work, low-noise melt pool definitions that tracked consistently with total melt pool size were identified; this is what is required for effective closed-loop control. Separate studies were conducted to characterize the interactions of primary process variables with melt pool size; an understanding of these interactions is critical for any monitoring, control, or quality assurance effort. These studies isolated each process variable individually and determined the melt pool response time on a limited basis, which will ultimately impact bandwidth capabilities for closed-loop control. Process transients were identified and characterized in both step changes in process parameters and in within-layer deposition trends. The interlayer melt pool size trend in the printing of a single bead wall was intriguing and highlighted the geometric effects that can be present, apart from thermal effects, that impact melt pool size. While there has been some exploration of this topic in the literature, further study of the factors, such as geometric influences on wetting angle, is warranted. Finally, the wire masking effect, or the blocking of the melt pool view by the wire at deposition angles near back feeding, was characterized, and a compensation algorithm was developed and successfully applied to generate a consistent melt pool size signal, which is an important contribution for control and quality assurance.

Acknowledgements

This research was funded by the U.S. Department of Energy, Office of Energy Efficiency and Renewable Energy, Advanced Manufacturing Office in partnership with GKN Aerospace. The authors gratefully acknowledge the extended Oak Ridge National Laboratory and GKN Aerospace teams that contributed to this work, including John Potter, Ronnie Wilson, and Chris Allison of GKN, as well as Abigail Barnes and Katherine Gaul of ORNL for manuscript review and editing. The authors also acknowledge Steffen Bonss of Laserline and Sandro Mehner of Fraunhofer USA for their advice and technical assistance.

References

[1] A. Heralic, A.K. Christiansson, K. Hurtig, M. Ottosson, B. Lennartson, Control design for automation of robotized laser metal-wire deposition, *Proceedings of the 17th World Congress of The International Federation of Automatic Control*, Seoul, Korea, July 6 - 11, 2008.

[2] T. Sentenac, Y. Le Maoult, G. Rolland, M. Devy, Temperature correction of radiometric and geometric models for an uncooled CCD camera in the near infrared, *IEEE Transactions on Instrumentation and Measurement*, Paper IM6224, pp. 1 - 18.

[3] A. Medrano, J. Folkes, J. Segal, I. Pashby, Fibre laser metal deposition with wire: Parameters study and temperature monitoring system, *Proceedings of SPIE; Presented at the XVII International Symposium on Gas Flow, Chemical Lasers, and High-Power Lasers*, Vol 7131, 2009.

[4] W. Tan, Y.C. Shin, Analysis of multi-phase interaction and its effects on keyhole dynamics with a multi-physics numerical model, *Journal of Physics D: Applied Physics*, Vol. 47, No. 34, 2014, pp. 1 - 17.

[5] L. Scime, J. Beuth, Using machine learning to identify in-situ melt pool signatures indicative of flaw formation in a laser powder bed fusion additive manufacturing process, *Additive Manufacturi*ng, Vol 25, 2019, pp. 151 - 165.

[6] G. Bi, A. Gasser, K. Wissenbach, A. Drenker, R. Poprawe, Identification and qualification of temperature signal for monitoring and control in laser cladding, *Optics and Lasers in Engineering*, Vol 44, 2006, pp. 1348 - 1359.

[7] D. Hu, H. Mei, G. Tao, R. Kovacevic, Closed loop control of 3d laser cladding based on infrared sensing, *Proceedings of the Solid Freeform Fabrication Symposium*, 2001, pp. 129 - 137.

[8] F. Meriaudeau, F. Truchetet, C. Dumont, E. Renier, P. Bolland, Acquisition and image processing system able to optimize laser cladding process, *Proceedings of ICSP*, 1996, pp. 1628 - 1631.

[9] J.M. Zalameda, E.R. Burke, R.A. Hafley, K.M.B. Taminger, C.S. Domack, A. Brewer, R.E. Martin, Thermal imaging for assessment of Electron-Beam Freeform Fabrication (EBF^3) additive manufacturing deposits, *Proceedings of SPIE; Presented in Thermosense: Thermal Infrared Applications XXXV*, Vol. 8705, 2013.

[10] M.L. Griffith, M.E. Schlienger, L.D. Harwell, M.S. Oliver, M.D. Baldwin, M.T. Ensz, J.E. Smugeresky, M. Essien, J. Brooks, C.V. Robino, W.H. Hofmeister, M.J. Wert, D.V. Nelson, Thermal behavior in the LENS process, *Proceedings of the Solid Freeform Fabrication Symposium*, 1998, pp. 89 - 96.

[11] W.H. Hofmeister, D.O. MacCallum, G.A. Knorovsky, Video monitoring and control of the LENS process, *Proceedings of the 9th International Conference of Computer Technology in Welding*, Detroit, MI, Sept. 28 – 30, 1999.

[12] W.H. Hofmeister, M. Griffith, M. Ensz, J. Smugeresky, Solidification in direct metal deposition by LENS processing, *JOM*, Sept. 2001, pp. 30 – 34.

[13] D. Hu, R. Kovacevic, Modelling and measuring the thermal behavior of the molten pool in closed-loop controlled laser-based additive manufacturing, *Proceedings of the Institution of Mechanical Engineers, Part B: Journal of Engineering Manufacture*, Vol. 217, 2003, pp. 441 – 452.

[14] P. Aggarangsi, J.L. Beuth, D.D. Gill, Transient changes in melt pool size in laser additive manufacturing process, *Proceedings of the Solid Freeform Fabrication Symposium*, 2004, pp. 163 - 174.

[15] P. Aggarangsi, J.L. Beuth, M. Griffith, Melt pool size and stress control for laser-based deposition near a free edge, *Proceedings of the Solid Freeform Fabrication Symposium*, 2003, pp. 196 - 207.

[16] J. Beuth, N. Klingbeil, The role of process variables in laser-based direct metal solid freeform fabrication, *JOM*, Sept. 2001, pp. 36 - 39.

[17] A. Birnbaum, P. Aggarangsi, J. Beuth, Process scaling and transient melt pool size control in laser-based additive manufacturing processes, *Proceedings of the Solid Freeform Fabrication Symposium*, 2003, pp. 328 – 339.

[18] S. Bonss, *Laserline*, Personal Communication, Aug. 22, 2018.

[19] D. Bristow, Melt pool measures and effective sensor bandwidth for direct energy deposition, *International Solid Freeform Fabrication Symposium*, Austin, TX, Aug. 12 - 14, 2019.